Vibration–rotation–tunneling dynamics calculations for the four-dimensional $(HCl)_2$ system: A test of approximate models

M. J. Elrod[a] and R. J. Saykally
Department of Chemistry, University of California, Berkeley, California 94720

(Received 26 October 1994; accepted 5 April 1995)

Several commonly used approximate methods for the calculation of vibration–rotation–tunneling spectra for $(HCl)_2$ are described. These range from one-dimensional models to an exact coupled four-dimensional treatment of the intermolecular dynamics. Two different potential surfaces were employed—an *ab initio* and our ES1 experimental surface (determined by imbedding the four-dimensional calculation outlined here in a least-squares loop to fit the experimental data, which is described in the accompanying paper [J. Chem. Phys. **103**, 933 (1995)]. The most important conclusion deduced from this work is that the validity of the various approximate models is extremely system specific. All of the approximate methods addressed in this paper were found to be sensitive to the approximate separability of the radial and angular degrees of freedom, wherein exists the primary difference between the two potentials. Of particular importance, the commonly used reversed adiabatic angular approximation was found to be very sensitive to the choice for fixed R; an improper choice would lead to results very much different from the fully coupled results and perhaps to false conclusions concerning the intermolecular potential energy surface. © *1995 American Institute of Physics.*

I. INTRODUCTION

The determination of intermolecular potential energy surfaces (IPS) from high resolution spectroscopy depends explicitly on the accuracy of the dynamical methods used to calculate such spectra from model potential surfaces. The spectra of weakly bound complexes (WBCs) are particularly difficult to calculate because most of the common simplifying assumptions used to interpret the spectra of covalently bound molecules are not applicable. The dynamics of WBCs are characterized by a hierarchy of nuclear motions. The intramolecular vibrations of the constituent monomers can usually be treated using a standard semirigid molecule analysis, but the coupling of these degrees of freedom to the intermolecular coordinates constitutes a much more difficult problem. For many systems of interest, however, the *intramolecular* vibrational frequencies are 1–2 orders of magnitude larger than the corresponding *intermolecular* frequencies, suggesting an adiabatic separation of these degrees of freedom. Because of the existence of multiple minima on the IPS as well as low barriers separating them, the intermolecular nuclear motions of WBCs are often characterized by strongly coupled and highly anharmonic dynamics that are often better described as tunneling motions or hindered internal rotation. The existence of such large amplitude dynamics suggests the applicability of a coordinate system which explicitly considers *all* possible intermolecular geometries. The use of such a global coordinate system (and an appropriate Hamiltonian) implies that none of the $3N$-6 (although the intramolecular degrees of freedom are often adiabatically separated) degrees of freedom are arbitrarily separable, and the full dimensionality of the dynamics problem must be retained. This situation represents a very serious escalation in computational cost; for a general dimer complex, the nonrotating intermolecular dynamics problem can involve up to six dimensions. For the typical case where ten basis functions are needed for each dimension, each added dimension represents a 100-fold increase in required memory and a 1000-fold increase in required CPU time when using standard direct diagonalization methods.

Because of these limitations, fully coupled intra- intermolecular dynamics calculations have been carried out only for a few simple systems.[1–3] In addition, calculations involving only the intermolecular degrees of freedom have been generally limited to systems with four dimensions or less, with the notable exceptions: CH_4H_2O,[4] Ar_2HCl,[5] $(NH_3)_2$,[6,7] and $(H_2O)_2$.[8,9] The systems for which such calculations have been used in conjunction with least-squares fitting of vibration–rotation–tunneling (VRT) spectroscopic data to determine improved intermolecular potential surfaces are[1,2,10,11] ArH_2, ArHF, ArHCl, ArH_2O, HeCO, and $ArNH_3$. By comparing the extensive spectroscopic literature for dimer systems to the much smaller body of theoretical work, it is quite apparent that calculations providing the necessary connection between the experimental data and the relevant intermolecular potential energy surfaces urgently need attention.

Although continuing advances in computational technology and the development of more efficient calculation methods are assured, the demand for calculations of increasingly higher dimension will always outstrip the ability to perform such calculations exactly. Because of this problem, approximate methods will continue to be important in the process of analyzing spectra in terms of the associated intermolecular potential energy surfaces. However, these approximate techniques must be used judiciously, since possible failures of these approaches can lead to erroneous conclusions about the potential surface of interest.

[a]Present address: Department of Earth, Atmospheric, and Planetary Sciences, Massachusetts Institute of Technology, 54-1312, Cambridge, MA 02139.

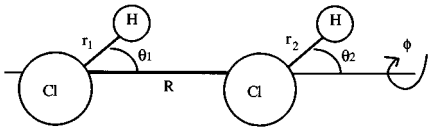

FIG. 1. Coordinate system for $(HCl)_2$.

It is the purpose of this paper to examine several widely used approximate methods—to compute the VRT dynamics—for the hydrogen-bonded $(HCl)_2$ system. We compare results from two different IPS describing the HCl–HCl interaction to demonstrate that the reliability of the various approximate techniques is strongly system dependent. One of these potentials was determined by *ab initio* methods[12,13] and has been previously used in a four-dimensional close-coupling calculation[14] of the $J=0$ states of $(HCl)_2$ as well in several of the approximate methods that will be described below. In this work, we extend the four-dimensional calculations on this *ab initio* surface to $J=1$ states and to the isotopomers $(DCl)_2$ and (HCl)(DCl) using an efficient variational method. In the accompanying paper (called II), the four-dimensional variational method described in this work is used to fit new and previously existing high resolution spectroscopic data for $(HCl)_2$ and $(DCl)_2$ to a new intermolecular potential energy surface (denoted ES1)—the second of the two potentials used in this work.

II. SPECTROSCOPIC NOMENCLATURE AND COORDINATE SYSTEM FOR $(HCl)_2$

For the purposes of discussing the VRT levels of $(HCl)_2$, it is necessary to adopt a notation to describe the intra- and intermolecular vibrations of the complex. The high frequency HCl stretching modes are denoted ν_1 and ν_2, for the ''free'' and ''bound'' monomers, respectively. For the intermolecular modes, the in-plane ''antigeared'' bending vibration is denoted ν_3, the intermonomer stretch is denoted ν_4, the in-plane ''geared'' bend is denoted ν_5, and the out-of-plane bend is denoted ν_6. The ν_5 mode correlates with the preferred very low barrier donor–acceptor interchange tunneling path, and the $\nu_5=0\rightarrow1$ energy difference can be identified as the tunneling splitting resulting from this process. An energy level diagram for $(HCl)_2$ is depicted in Fig. 1. The intermolecular eigenstates are labeled with the following notation: $|\nu_3\nu_4\nu_5\nu_6\rangle$. It is also useful to classify the VRT levels according to their irreducible representation in the $C_{2h}(M)$ molecular symmetry group (see Table I for character table). The electric dipole selection rules require $A\leftrightarrow A$ or $B\leftrightarrow B$ and $+\leftrightarrow-$. The four-dimensional intermolecular coordinate system for $(HCl)_2$ is depicted in Fig. 2. The *ab initio* equilibrium structure for $(HCl)_2$ is $R=3.82$ Å $\theta_1=7.4°$ $\theta_2=87.7°$ $\phi=180°$ with an absolute well depth of 626 cm^{-1}.

TABLE I. Character table for $C_{2h}(M)$ molecular symmetry group.

Γ	E	(12)	E^*	(12)*
A^+	1	1	1	1
A^-	1	1	−1	−1
B^+	1	−1	1	−1
B^-	1	−1	−1	1

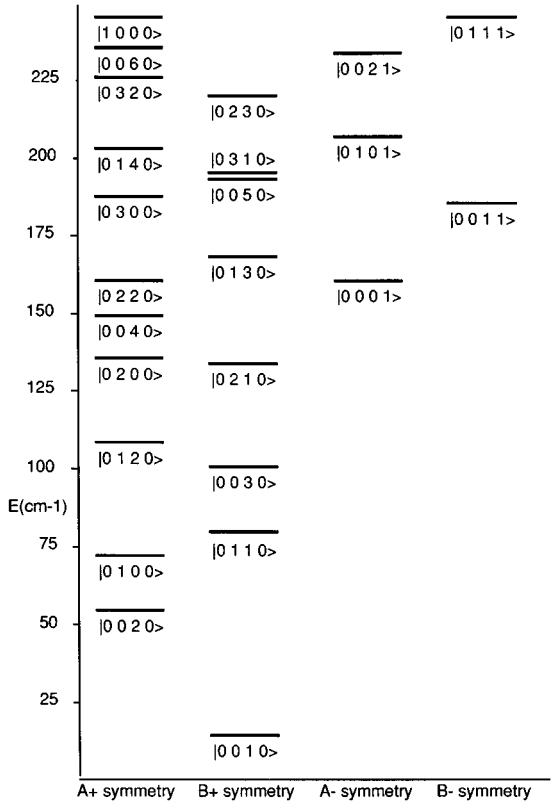

FIG. 2. Energy level diagram (states labeled by $|\nu_3\nu_4\nu_5\nu_6\rangle$) for $(HCl)_2$.

In order to facilitate the calculation of the angular matrix elements in the space-fixed coupling scheme, the intermolecular potential energy surface is expressed in a single center spherical expansion:

$$V(r_1,r_2,R,\theta_1,\theta_2,\phi)=\sum_{l_1l_2l} A_{l_1l_2l}(R,r_1,r_2)g_{l_1l_2l}(\theta_1,\theta_2,\phi). \tag{1}$$

The basis functions, $g_{l_1l_2l}(\theta_1,\theta_2,\phi)$, and the potential coefficients, $A_{l_1l_2l}(R,r_1,r_2)$, are defined in Paper II for both the *ab initio* and the experimental ES1 potential energy surfaces.

III. DESCRIPTION OF APPROXIMATE METHODS

In general, *ab initio* studies often report vibrational frequencies obtained by numerically differentiating the energy with respect to the proper coordinates to find the harmonic force constants. However, the use of this approximation involves the assumption of both harmonicity and separability. Since the assumption of harmonicity for weakly bound complexes is known to be entirely inadequate, these calculations can usually only be considered qualitatively useful, and we therefore do not address them in this analysis. We also do not address the effects of adiabatically separating the intra- and intermolecular degrees of freedom. The *ab initio* potential[13] for $(HCl)_2$ predicts that the H—Cl bond length changes by only 0.001 Å along the donor–acceptor interchange tunneling path. This corresponds to a total energy change of only

TABLE II. Physical data used in all calculations.

	Atomic mass (amu)	r (Å)	b (cm^{-1})
H	1.007 825		
D	2.014 102		
^{35}Cl	34.968 85		
$H^{35}Cl$		1.278	10.4400
$D^{35}Cl$		1.278	5.3923

0.05 cm^{-1}, which is far smaller than the quantitative precision available with the current theoretical approach. Thus, the adiabatic separation of the intramolecular coordinates is expected to be an excellent approximation for the calculation of intermolecular energies for the $(HCl)_2$ system in particular.

We focus instead on the intermolecular dynamics of $(HCl)_2$, with a view towards elucidating the issue of the approximate separability of coordinates. In particular, we discuss the separation of the large amplitude donor–acceptor interchange tunneling coordinate from the other intermolecular degrees of freedom using the semirigid bender model. We also examine the reversed adiabatic approximation, which allows a separation of the radial and angular degrees of freedom into individual dynamics problems of one and three dimensions, respectively. This approximation, in particular, has been widely used for the hydrogen bonded dimer systems[8,15–17] despite the troubling fact that the stretching and bending modes oscillate on comparable time scales. We also address the helicity decoupling approximation (the neglect of Coriolis coupling terms), which can be utilized for calculations using body-fixed coordinates. The calculation of spectra for the isotopomers of $(HCl)_2$ are also discussed, as the shift in the center-of-mass based coordinate system complicates the dynamics calculations. The effects of neglecting this shift are discussed. Calculations at all levels of approximation were performed with fixed HCl bond lengths, and the relevant physical constants (bond lengths, atomic masses, and HCl rotational constants) are contained in Table II. In order to compare with previous calculations,[14] we adopt the procedure of using the *experimentally* determined rotational constant (B_0), while fixing the HCl bond lengths at their *ab initio* equilibrium values (r_e). Although this procedure is inconsistent, since it is formally proper to use the *average* bond lengths (and B_0), it ensures an ''experimentally'' accurate evaluation of the intermolecular kinetic energy (which depends greatly on B_0) while providing a more consistent connection to the theoretically generated potential energy surface. In any case, the *intermolecular* potential energy surface is only weakly dependent on the HCl bond length for the small differences involved.

IV. THE SEMIRIGID BENDER: A ONE-DIMENSIONAL TUNNELING APPROXIMATION

In the widely used semirigid bender technique,[13,18–23] one large amplitude coordinate is treated rigorously, and the other degrees of freedom are allowed to change parametrically as the molecule executes this effective one-dimensional motion. Using this treatment, the calculation for the large amplitude geared $[(\theta_1+\theta_2)/2]$ donor–acceptor interchange coordinate in $(HCl)_2$ is recast into a one-dimensional ''tunneling coordinate'' problem. The angular coordinates ρ and σ are defined as

$$\rho=(\theta_1+\theta_2)/2, \tag{2}$$

$$\sigma=(\theta_1-\theta_2)/2, \tag{3}$$

where $0°\leqslant\rho\leqslant180°$. Given the complete IPS and an effective tunneling potential ($V_{\min}$), σ and R are expanded in terms of ρ to fit this tunneling pathway. Bunker *et al.* used a $V_{\min}$ fitted to points from the *ab initio* potential[14] to calculate the tunneling levels of $(HCl)_2$ and $(DCl)_2$ via the semirigid bender approach.[13] The following expressions were obtained for $V_{\min}$, σ, and R:

$$\begin{aligned}V_{\min}(cm^{-1})=&230-375.5\sin\rho-113.1\sin^2\rho\\&+158.2\sin^3\rho+121.3\sin^4\rho\\&+44.2\sin^5\rho,\end{aligned} \tag{4}$$

$$\begin{aligned}\sigma(\text{deg})=&39.25-1.37\sin\rho+1.75\sin^2\rho\\&-13.28\sin^3\rho+22.19\sin^4\rho\\&+10.96\sin^5\rho-16.74\sin^6\rho,\end{aligned} \tag{5}$$

and

$$\begin{aligned}R(\text{Å})=&(3.8616/2)\{1-\tanh[0.3(\rho-46.11)]\}\\&+(3.8616/2)\{1-\tanh[0.3(180-46.11-\rho)]\}\\&+(3.8070/4)\{1-\tanh[0.3(46.11-\rho)]\}\\&\times\{1-\tanh[0.3(\rho-180+46.11)]\}.\end{aligned} \tag{6}$$

The experimental ES1 $(HCl)_2$ potential described in Paper II was similarly fit to potential points along the donor–acceptor interchange tunneling pathway to obtain $V_{\min}$, σ, and R:

$$\begin{aligned}V_{\min}(cm^{-1})=&278-414.5\sin\rho-104.9\sin^2\rho\\&-42.5\sin^3\rho+273.2\sin^4\rho\\&+213.9\sin^5\rho-151.7\sin^6\rho,\end{aligned} \tag{7}$$

$$\begin{aligned}\sigma(\text{degrees})=&40.93+7.78\sin\rho-5.78\sin^2\rho\\&-40.15\sin^3\rho+35.91\sin^4\rho\\&+26.31\sin^5\rho-22.23\sin^6\rho,\end{aligned} \tag{8}$$

and

$$\begin{aligned}R(\text{Å})=&3.73+0.24\sin\rho-0.09\sin^2\rho-0.96\sin^3\rho\\&+0.87\sin^4\rho+0.65\sin^5\rho-0.79\sin^6\rho.\end{aligned} \tag{9}$$

The semirigid bender Hamiltonian for $(HCl)_2$ is

$$\widehat{H_{\text{srb}}}=\frac{\hbar^2\mu_{\rho\rho}\partial^2}{2\partial\rho^2}+\frac{\hbar^2\mu_{zz}K^2}{2}+V_{\min}(\rho), \tag{10}$$

where $\mu_{\rho\rho}$ and μ_{zz} are the coordinate-dependent inverse moments of inertia.[24] In most applications of this method, the Schrödinger equation is solved via the Numerov–Cooley algorithm.[21] In our application of the method, we chose to use a basis set method (distributed Gaussian functions)[25] to solve the differential equation. A basis set of 100 distributed

Gaussian functions yielded energies converged to better than 0.001 cm^{-1} for the states of interest. The transition moments and rotational constants can also be calculated from the resulting eigenvectors,[24] although these properties are not of interest in the present context.

V. REVERSED ADIABATIC APPROXIMATION: 1D RADIAL PROBLEM

The one-dimensional dynamics calculation for the van der Waals stretching states is easily accomplished with modern computational methods and technology. However, since the fully coupled calculations described in a following section employ radial basis sets which have been preconditioned (contracted) by solving a one-dimensional problem which closely mimics the radial potential of the 4D IPS, we discuss these techniques in more detail. The radial part of the Hamiltonian can be simply written

$$\widehat{H_{\text{rad}}} = \frac{\hbar^2 \partial^2}{2\mu \partial R^2} + V_{\text{eff}}(R). \tag{11}$$

There are several possible choices for $V_{\text{eff}}(R)$. The most common approach is to fix the other degrees of freedom at their equilibrium values to determine $V_{\text{eff}}(R)$ from the full IPS. For $(HCl)_2$, it is a better approximation to fix the angular degrees of freedom at the C_{2h} saddle point in order to approximately take into account the vibrational averaging resulting from the large amplitude donor–acceptor interchange tunneling. This effective one-dimensional potential surface is denoted $V_{\text{eff}}^{\text{cut}}(R)$. Using a 16 function harmonic oscillator basis (with variationally optimized α and r_e parameters) and a 24 point Gauss–Hermite numerical integration scheme, we performed a calculation of this kind for both potential surfaces. This method is obviously quite inaccurate for systems which carry out large amplitude excursions from their equilibrium geometries.

A more rigorous method for generating an effective one-dimensional potential involves solving the angular part of the problem exactly (which will be described in the next section) as a function of R and using the lowest eigenvalue at each R to construct the radial potential, denoted $V_{\text{eff}}^{\text{ang}}(R)$. Thus, the effects of vibrational averaging over the large amplitude angular coordinates are thereby treated rigorously as opposed to the simple one-dimensional cut through the total potential surface described in the preceding paragraph. In the limit of *no* coupling between the angular and radial degrees of freedom, this approach would yield *exact* eigenvalues. Since three of the four intermolecular coordinates for $(HCl)_2$ are angles, this approach is almost as time consuming as performing the full 4D calculation, although important reductions in the basis set size can be achieved.

VI. REVERSED ADIABATIC APPROXIMATION: 3D ANGULAR PROBLEM

Since most of the complexity of the full IPS for many systems of current interest is contained in the angular degrees of freedom and since the strongest VRT transitions involve states which are also associated with these coordinates, many calculations aimed at rationalizing spectroscopic data utilize effective angular approximations. Althorpe *et al.*[15] reported calculations of this kind for $(HF)_2$, $(HCl)_2$, and $(HBr)_2$. The effective angular Hamiltonian (which depends parametrically on R) written in a space-fixed angular momentum coupling scheme is

$$\hat{H}_{\text{ang}} = b_1 \hat{j}_1^2 + b_2 \hat{j}_2^2 + \frac{\hbar^2 l^2}{2\mu R^2} + V(R, \theta_1, \theta_2, \phi). \tag{12}$$

Here μ is the reduced mass of the complex, b_1 and b_2 are the rotational constants of monomers 1 and 2, $\hat{j}_1^2$ and $\hat{j}_2^2$ are the rotational angular momentum operators for monomers 1 and 2, $\hat{l}^2$ is the orbital angular momentum operator associated with the end-over-end rotation of the complex, and $V(R,\theta_1,\theta_2,\phi)$ is the intermolecular potential energy function. The appropriate space-fixed angular basis is of the form[26]

$$\begin{aligned} |j_1 j_2 j_{12} l J M\rangle &= \sum_{m_1 m_1 m_{12} n} Y_{j_1 m_1}(\theta_1, \phi_1) Y_{j_2 m_2}(\theta_2, \phi_2) Y_{ln}(\theta, \phi) \\ &\quad \times \langle j_1 m_1, j_2 m_2 | j_{12} m_{12} \rangle \langle j_{12} m_{12}, ln | J M \rangle, \end{aligned} \tag{13}$$

where $Y_{j_1 m_1}(\theta_1, \phi_1)$ is a spherical harmonic and $\langle j_1 m_1, j_2 m_2 | j_3 m_3 \rangle$ is a Clebsch–Gordan coefficient.[27] In the space-fixed coupling scheme, j_1 and j_2 are coupled to give j_{12} which is subsequently coupled with l to give J, the total angular momentum of the system. Only J and M are conserved quantities in this scheme. The basis set is truncated by considering only j_1 and $j_2 \leqslant j_{\max}$.

The effects of the permutation–inversion operators from the $C_{2h}(M)$ molecular symmetry group on the space-fixed coordinates are listed in Table III. From this information, linear combinations of the basis functions which transform as the irreducible representations of $C_{2h}(M)$ can be constructed in order to partition the Hamiltonian matrix into four noninteracting subblocks

$$\begin{aligned} |j_1 j_2 j_{12} l p J M\rangle = \frac{1}{\sqrt{2(1+\delta_{j_1 j_2})}} [&|j_1 j_2 j_{12} l J M\rangle \\ &+ (-1)^{j_1 + j_2 + j_{12} + l + p} |j_2 j_1 j_{12} l J M\rangle]. \end{aligned} \tag{14}$$

Functions with $p=0$ and j_1+j_2+1 even span the A^+ irreducible representation. Similarly $p=0$; j_1+j_2+l odd, $p=1$; j_1+j_2+l even, and $p=1$; j_1+j_2+l odd span the A^-, B^+, and B^- irreducible representations, respectively.

The angular kinetic energy matrix elements may be easily evaluated in this basis

TABLE III. Effect of $C_{2h}(M)$ permutation–inversion operators on coordinates.

E	(12)	E^*
θ_1, ϕ_1	θ_2, ϕ_2	$\pi-\theta_1, \phi_1+\pi$
θ_2, ϕ_2	θ_1, ϕ_1	$\pi-\theta_2, \phi_2+\pi$
θ, ϕ	$\pi-\theta, \phi+\pi$	$\pi-\theta, \phi+\pi$

$$\langle j_1 j_2 j_{12} lJM|T|j_1' j_2' j_{12}' l' JM\rangle = \left[b_1 j_1(j_1+1) + b_2 j_2(j_2+1) + \frac{\hbar^2}{2\mu R^2} l(l+1) \right] \times \delta_{j_1,j_1'} \delta_{j_2,j_2'} \delta_{j_{12},j_{12}'} \delta_{l,l'}. \quad (15)$$

In this formalism, it is convenient to expand the intermolecular potential similarly [as defined in Eq. (1)], since the resulting integrals of the potential over the angular basis set are then analytic[26]

$$\langle j_1 j_2 j_{12} lJM|V|j_1' j_2' j_{12}' l' JM\rangle = \sum_{\mathbf{l}_1 \mathbf{l}_2 \mathbf{l}} A_{l_1 l_2 l}(R)(-1)^{J+j_1+j_2+j_{12}'} \times \left(\frac{[j_1][j_2][j_{12}][l][j_1'][j_2'][j_{12}'][l'][\mathbf{l}_1][\mathbf{l}_2][\mathbf{l}]^2}{(4\pi)^3} \right)^{1/2} \times \begin{pmatrix} l & \mathbf{l} & l' \\ 0 & 0 & 0 \end{pmatrix} \begin{pmatrix} j_1 & l_1 & j_1' \\ 0 & 0 & 0 \end{pmatrix} \begin{pmatrix} j_2 & \mathbf{l}_2 & j_2' \\ 0 & 0 & 0 \end{pmatrix} \times \begin{Bmatrix} l & \mathbf{l} & l' \\ j_{12}' & J & j_{12} \end{Bmatrix} \begin{Bmatrix} j_{12}' & j_2' & j_1' \\ j_{12} & j_2 & j_1 \\ \mathbf{l} & \mathbf{l}_2 & \mathbf{l}_1 \end{Bmatrix}, \quad (16)$$

where $[j]=2j+1$, the 2 by 3 matrices in parenthesis and braces are Wigner 3-j and 6-j symbols, respectively, and the 3 by 3 matrix in braces is a Wigner 9-j symbol.[27] The quantum numbers associated with the expansion of the potential are denoted in bold type in order to prevent confusion with the end-over-end rotational quantum number associated with the angular basis.

In addition to energy calculations, this choice for the angular basis also makes the calculation of other important properties efficient. From experimental measurements of dipole moments and nuclear quadrupole coupling constants, the angular expectation values—$\langle P_1(\cos\theta)\rangle$ and $\langle P_2(\cos\theta)\rangle$—can be obtained. However, since the donor–acceptor interchange tunneling is much faster than the end-over-end rotation for symmetric $[H(D)Cl]_2$ complexes, $\langle P_1(\cos\theta_1)\rangle + \langle P_1(\cos\theta_2)\rangle = 0$. Matrix elements [i.e., $\mathbf{l}_1=2$, $\mathbf{l}_2=0$, and $\mathbf{l}=2$ for $\langle P_2(\cos\theta_1)\rangle$] are calculated in the determination of the energies, so the calculation of these expectation values is a simple sum as dictated by the coefficients of the relevant eigenvector. For the purposes of assigning states in the calculation of spectra for the mixed dimer (HCl)(DCl), these expectation values are invaluable.

The transition intensities may also be easily calculated in this scheme by assuming that the dipole moment of the dimer is approximated by a vector sum of the two monomer moments[15]

$$\langle \mu^1_{i\to f}\rangle + \langle \mu^2_{i\to f}\rangle = \langle j_1 j_2 j_{12} lJM|P_1(\cos\theta_1) + P_1(\cos\theta_2)|j_1' j_2' j_{12}' l' J' M'\rangle, \quad (17)$$

where

$$\langle \mu^1_{i\to f}\rangle = \delta_{j_2,j_2'} \delta_{l,l'} (-1)^{j_1+j_1'+j_2+j_{12}+j_{12}'+l+M'} \times \left(\frac{3[j_1][j_1'][j_{12}][j_{12}'][J][J']}{4\pi} \right)^{1/2} \begin{pmatrix} j_1 & 1 & j_1' \\ 0 & 0 & 0 \end{pmatrix} \times \begin{pmatrix} J & 1 & J' \\ M & 0 & -M' \end{pmatrix} \begin{Bmatrix} j_{12} & 1 & j_{12}' \\ j_1' & j_2 & j_1 \end{Bmatrix} \times \begin{Bmatrix} J & 1 & J' \\ j_{12}' & l & j_{12} \end{Bmatrix}. \quad (18)$$

This expression imposes the usual rotational selection rules ($\Delta J=0, \pm1$, $\Delta M=0$), but the selection rules imposed by symmetry ($A\leftrightarrow A$, $B\leftrightarrow B$, $+\leftrightarrow -$) must also be considered. The relative absorption intensities $[I(\omega)]$ can be calculated from[28]

$$I(\omega) \propto \omega g'' [e^{(-E''/kT)} - e^{(-E'/kT)}][\langle \mu^1_{i\to f}\rangle + \langle \mu^2_{i\to f}\rangle]^2, \quad (19)$$

where $\omega = E' - E''$ and g'' is the degeneracy of the initial state.

VII. FULLY COUPLED FOUR-DIMENSIONAL VARIATIONAL APPROACH

The four-dimensional treatment of the intermolecular dynamics is approximate only in neglecting the coupling of the high frequency H–Cl stretching vibrations to the intermolecular modes. The four-dimensional technique simply involves the extension of the angular approximation to include the radial coordinate. The full intermolecular Hamiltonian is then

$$\hat{H} = \frac{\hbar^2 \partial^2}{2\mu \partial R^2} + b_1 \hat{j}_1^2 + b_2 \hat{j}_2^2 + \frac{\hbar^2 \hat{l}^2}{2\mu R^2} + V(R, \theta_1, \theta_2, \phi), \quad (20)$$

where the components of the Hamiltonian are defined above. The corresponding matrix elements are

$$\langle n|\langle j_1 j_2 j_{12} lJM|\hat{H}|j_1' j_2' j_{12}' l' JM\rangle|n'\rangle = [b_1 j_1(j_1+1) + b_2 j_2(j_2+1)]\delta_{j_1,j_1'}\delta_{j_2,j_2'}\delta_{j_{12},j_{12}'}\delta_{l,l'}\delta_{n,n'} + \langle n|\left[\frac{\hbar^2}{2\mu}\frac{\partial^2}{\partial R^2} + \frac{\hbar^2}{2\mu R^2} l(l+1)\right] \times \delta_{j_1,j_1'}\delta_{j_2,j_2'}\delta_{j_{12},j_{12}'}\delta_{l,l'} + \langle j_1 j_2 j_{12} lJM|V(R)|j_1' j_2' j_{12}' l' JM\rangle|n'\rangle, \quad (21)$$

where n represents the radial basis index. In order to keep the Hamiltonian matrix size manageable, two radial basis contraction schemes were implemented. In these contraction methods, a model one-dimensional problem is solved and the resulting eigenfunctions are used for the radial basis in the fully coupled problem. The contraction schemes are then differentiated only by the choice of $V_{\text{eff}}(R)$. The two methods used here are those described in the previous section on one-dimensional radial approximations. Since the *ab initio* potential is characterized by relatively small angular–radial coupling, the effective potential $[V_{\text{eff}}^{\text{ang}}(R)]$ generated by the solution of the angular problem at several values of R is a

very accurate description of the true radial potential and the resulting eigenfunctions are very close to the fully coupled radial eigenfunctions. We used this method for the calculation of properties from the *ab initio* potential. However, the calculations using the experimental ES1 potential described in Paper II utilized the fast, simple fixed-angles method [using $V_{\mathrm{eff}}^{\mathrm{cut}}(R)$] because the increased degree of angular–radial coupling in the experimentally determined potential made the $[V_{\mathrm{eff}}^{\mathrm{ang}}(R)]$ method too inefficient to justify its computational cost. The numerical integration over the radial basis in the coupled problem is accomplished by a 16 point Gauss–Hermite quadrature (harmonic oscillator functions are used in the primitive basis, such that the differential kinetic operator matrix element can be evaluated analytically).

VIII. HELICITY DECOUPLING APPROXIMATION

In a body-fixed formalism, it is possible to neglect contributions to the total energies from Coriolis coupling—the ''helicity decoupling'' approximation—in order to keep the matrix size independent of the total angular momentum quantum number. The space-fixed formalism, which is used here, does not allow this simplifying approximation. In order to assess whether the usefulness of this approximation could suggest the superiority of the body-fixed method, we compared the explicit $J=0\rightarrow1$ spacings (which include the effects of Coriolis coupling) with values estimated from the expectation value of $1/R^2$. The value of $\langle 1/R^2\rangle$ was computed by direct numerical integration over the radial coordinate using the eigenvectors from the full dynamical calculation. It was found that the energy differences varied on average (for the states of interest) by about 0.001 cm^{-1} and some higher lying states showed differences as much as 0.004 cm^{-1}. Since the important effects of angular–radial coupling resulted in energy shifts of this order, the helicity decoupling approximation is not appropriate for a completely quantitative calculation of the $(HCl)_2$ eigenstates. Therefore, since the full dynamics must be treated to obtain adequate quantitative results, the efficiency of the calculation method is not dictated by the choice of body- or space-fixed coordinates, at least in this case, since the matrix setup steps dominate the required CPU time.

IX. CONVERGENCE OF THE FOUR-DIMENSIONAL BASIS SET

The convergence of the basis set expansion is a particularly important issue in a consideration of the feasibility of performing a least-squares fit to experimental data (as described in Paper II), as the size of the basis directly influences the required CPU time (as well as the obvious memory limitations). It should also be noted that the $(HCl)_2$ surface is significantly more anisotropic than the previously studied systems of lower dimensionality (Ar-molecule). This property will inevitably result in slower angular basis convergence. In Table IV, we list the ground state energies and several relevant energy differences as a function of the angular basis set size ($j_{\max}$) for the $(HCl)_2$ *ab initio* potential. The rate of convergence for each vibrational level is rationalized by the position of the eigenstate in the in-plane region of the potential: the slowest converging state is the antigeared in-plane bending vibration ($|1\ 0\ 0\ 0\rangle$) at 220 cm^{-1}. Reference to Table IV reveals that, for the *ab initio* potential, basis set sizes of $j_{\max}=8$ are sufficient to converge all experimentally accessed vibrational states to $\sim$0.1 cm^{-1}.

TABLE IV. Angular convergence properties for $(HCl)_2$ using *ab initio* (Ref. 13) potential (energies in cm^{-1} and relative to ground state).

$j_{\max}$	Ground state	$\|0\ 0\ 1\ 0\rangle$	$\|0\ 0\ 2\ 0\rangle$	$\|0\ 0\ 3\ 0\rangle$	$\|0\ 0\ 0\ 1\rangle$	$\|1\ 0\ 0\ 0\rangle$
5	−368.735	14.506	61.929	107.294	140.508	231.657
6	−371.108	13.248	61.066	101.394	139.567	224.028
7	−371.632	12.782	59.854	99.848	139.004	221.392
8	−371.773	12.690	59.735	99.414	138.866	220.379
9	−371.804	12.669	59.691	99.335	138.833	220.172
10	−371.810	12.665	59.683	99.316	138.827	220.124
11	−371.811	12.664	59.682	99.312	138.826	220.115
12	−371.811	12.664	59.681	99.312	138.826	220.113

[a]Using one radial basis function.

Because of the small angular–radial coupling evident in the *ab initio* surface and the fact that none of the van der Waals stretching vibrations had been experimentally measured, it was hoped that relatively small radial basis sets could be successfully implemented so as to keep the total basis small enough to allow the eigenvalue routine to be embedded in a least-squares iterative loop. As described above in the radial approximations section, two different ''contracted'' radial basis sets [formed by solving the one-dimensional radial problem using either $V_{\mathrm{eff}}^{\mathrm{cut}}(R)$ or $V_{\mathrm{eff}}^{\mathrm{ang}}(R)$ as effective potentials] were used. In Tables VA and VB, the convergence properties for the contracted radial basis formed from $V_{\mathrm{eff}}^{\mathrm{cut}}(R)$ are presented. Similarly, the convergence results for the basis formed from $V_{\mathrm{eff}}^{\mathrm{ang}}(R)$ are presented in Tables VIA and VIB. Although the ''ang'' basis converges the vibrational origins to a *satisfactory* level of accuracy extremely quickly, the ''cut'' basis actually converges to a *high* level of accuracy faster. As was pointed out by LeRoy *et al.*,[29] it is often counterproductive to obtain highly accurate eigenvectors from a basis set contraction, since these functions may not contain enough flexibility to handle the difference between the one-dimensional and four-dimensional potentials. Therefore, the ang basis is superior only in situations where the radial basis must be kept extremely small. In order to achieve satisfactory convergence in both the angular and radial coordinates, limitations on computer resources will determine this choice. For the $(HCl)_2$ *ab initio* potential, the ang basis is preferable for radial basis set sizes of three or less and the cut basis is preferable for basis set sizes of four or more. The $J=0\rightarrow1$ energy differences, which are the only available experimental observables which directly depend on the radial coordinate, are less sensitive to the differences in the two basis sets than are the energies of the vibrational eigenstates. For the calculations on the *ab initio* potential, a basis set size of $j_{\max}=9$ and $n=3$ (for $J=0$ and 1) was chosen as the best compromise to produce the most accurate eigenvalues and the ang radial basis set was therefore chosen. However, in the course of the fitting of a new experimental potential described in the accompanying paper, a basis set size of $j_{\max}=8$ and $n=4$ was used with the

TABLE V. Radial basis set [using $V_{\text{eff}}^{\text{cut}}(R)$] convergence properties for selected vibrational levels of $(HCl)_2$ using *ab initio* (Ref. 13). potential (energies in cm^{-1}).

A. Vibrational levels (relative to the ground state)

n[a]	Ground state	$\|0\ 1\ 0\ 0\rangle$	$\|0\ 2\ 0\ 0\rangle$	$\|0\ 0\ 1\ 0\rangle$	$\|0\ 0\ 2\ 0\rangle$	$\|0\ 0\ 0\ 1\rangle$
1	−363.598			15.608	62.906	144.108
2	−369.848	59.011		14.278	63.110	138.332
3	−369.931	48.180	113.610	14.274	61.295	137.225
4	−369.933	47.890	92.688	14.274	61.275	137.185
5	−369.933	47.886	92.012	14.274	61.275	137.184
6	−369.933	47.886	92.003	14.274	61.275	137.184

B. $J=0\rightarrow1$ spacings

n[a]	Ground state	$\|0\ 1\ 0\ 0\rangle$	$\|0\ 2\ 0\ 0\rangle$	$\|0\ 0\ 1\ 0\rangle$	$\|0\ 0\ 2\ 0\rangle$	$\|0\ 0\ 0\ 1\rangle$
1	0.126 57			0.126 49	0.126 71	0.126 93
2	0.121 22	0.125 10		0.120 76	0.123 07	0.119 77
3	0.120 99	0.117 22	0.124 72	0.120 52	0.120 13	0.118 00
4	0.121 00	0.116 40	0.113 70	0.120 52	0.120 10	0.117 87
5	0.121 00	0.116 40	0.111 86	0.120 52	0.120 10	0.117 87
6	0.121 00	0.116 40	0.111 84	0.120 52	0.120 10	0.117 86

[a]Using an angular basis with $j_{\max}=5$.

cut radial basis set to produce optimal results. It should also be pointed out that the ease of determining of the cut basis set at each least-squares iteration was also an important consideration in this choice.

X. SINGLE-CENTER SPHERICAL EXPANSION OF THE POTENTIAL

In their fitting of the $(HCl)_2$ *ab initio* analytical potential, Bunker *et al.*[13] used the single-center spherical expansion formalism so that it could directly incorporated into the kind of calculations described here. To make such variational methods feasible, it is crucial for the potential to be of this form so that the integrals of the potential over the angular basis set are analytic. In our application, this is important for two important purposes. First, as we described above, this is the same general approach one would use to perform calculations on a potential of a general form. In the accompanying paper, we use this formalism to express a previously reported semiempirical $(HCl)_2$ potential[30] (which is cast in a site–site coordinate system) in the single center spherical expansion and to perform dynamical calculations in order to facilitate comparison to the other available potential surfaces. Second, these considerations are necessary in order to rigorously calculate spectra for $(DCl)_2$ and (HCl)(DCl) from the available potential surfaces for $(HCl)_2$. Although the Born–Oppenheimer approximation is assumed here [i.e., $(HCl)_2$ and $(DCl)_2$ possess the same potential surface], it is necessary to retain a center-of-mass based angular coordinate system so that the angular kinetic energy operators retain their simple form. Therefore, this requires that coordinate system be shifted to the DCl centers of mass, resulting in new values for the angular coefficients.

In their paper describing approximate calculations for $(DCl)_2$ using a purely electrostatic (dipole and quadrupole

TABLE VI. Radial basis set [using $V_{\text{eff}}^{\text{ang}}(R)$] convergence properties for selected vibrational levels of $(HCl)_2$ using *ab initio* (Ref. 13) potential (energies in cm^{-1}).

A. Vibrational levels (relative to the ground state)

n[a]	Ground state	$\|0\ 1\ 0\ 0\rangle$	$\|0\ 2\ 0\ 0\rangle$	$\|0\ 0\ 1\ 0\rangle$	$\|0\ 0\ 2\ 0\rangle$	$\|0\ 0\ 0\ 1\rangle$
1	−369.554			14.297	61.275	138.869
2	−369.894	48.626		14.273	61.335	137.202
3	−369.915	47.957	93.134	14.276	61.287	137.174
4	−369.922	47.919	92.132	14.277	61.278	137.177
5	−369.925	47.901	92.061	14.276	61.275	137.179
6	−369.927	47.890	92.031	14.275	61.274	137.181

B. $J=0\rightarrow1$ spacings

n[a]	Ground state	$\|0\ 1\ 0\ 0\rangle$	$\|0\ 2\ 0\ 0\rangle$	$\|0\ 0\ 1\ 0\rangle$	$\|0\ 0\ 2\ 0\rangle$	$\|0\ 0\ 0\ 1\rangle$
1	0.121 10			0.121 04	0.121 25	0.121 45
2	0.120 97	0.116 64		0.120 52	0.120 13	0.117 98
3	0.120 99	0.116 34	0.112 62	0.120 51	0.120 06	0.117 81
4	0.120 99	0.116 37	0.111 74	0.120 51	0.120 08	0.117 82
5	0.121 00	0.116 37	0.111 77	0.120 52	0.120 09	0.117 81
6	0.121 00	0.116 38	0.111 79	0.120 52	0.120 10	0.117 81

[a]Using an angular basis with $j_{\max}=5$.

moments only) surface, Schuder *et al.*[17] treated this coordinate shift incorrectly. Although they correctly noted that the dipole moment of HCl does not depend on the *molecular* origin, they neglected to consider the fact that the dipole–dipole *interaction* (or multipole–multipole interaction, in general) *is* origin dependent. Therefore, the DCl center-of-mass based coordinate system has no direct relationship to the HCl center-of-mass system and must be determined by a rigorous transformation in the same general sense as would be necessary for a potential expressed in a completely different coordinate system. In practice, the coordinate transformation, $\{R,\theta_1,\theta_2,\phi\}^{\mathrm{DCl}}\rightarrow\{R,\theta_1,\theta_2,\phi\}^{\mathrm{HCl}}$, is performed by first transforming to Cartesian coordinates and then transforming back to spherical coordinates in the new reference frame. It is necessary to transform from the DCl to the HCl reference frames, since the potential energy is known only in the HCl-based coordinate system. The DCl-based potential coefficients are then generated as described in the following paragraph. It should also be pointed out that the adiabatic separation of the *intramolecular* coordinates will lead to small differences in the HCl or DCl averaged *intermolecular* angular coefficients, but these effects on the energies are estimated to be much smaller than the errors due to basis set truncation.

In order to determine the angular coefficients, the potential of interest is projected onto the angular basis functions

$$A_{l_1l_2l}(R)=\int_0^{2\pi}\int_0^{\pi}\int_0^{\pi}V(\theta_1,\theta_2,\phi;R)g_{l_1l_2l}\times(\theta_1,\theta_2,\phi)\sin\theta_1\sin\theta_2\,d\phi d\theta_1 d\theta_2, \quad (22)$$

such that for sufficient values of $\mathbf{l}_1^{\max}$ and $\mathbf{l}_2^{\max}$ the following expression holds:

$$V(R,\theta_1,\theta_2,\phi)=\sum_{l_1l_2l}A_{l_1l_2l}(R)g_{l_1l_2l}(\theta_1,\theta_2,\phi). \quad (23)$$

The basis function $g_{\mathbf{l}_1\mathbf{l}_2\mathbf{l}}(\theta_1,\theta_2,\phi)$ is defined in the accompanying paper and the integration over ϕ is performed using an 8 point Gauss–Chebyshev quadrature and the integration over θ_1 and θ_2 is performed using a 6 point Gauss–Legendre quadrature for each angle. In practice, the $A_{\mathbf{l}_1\mathbf{l}_2}(R)$ coefficients are not fit to an explicit R-dependent form but are determined for each quadrature point in the integration over the radial basis (usually 16 Gauss–Hermite points). For an expansion up to $\mathbf{l}_1^{\max}=\mathbf{l}_2^{\max}=5$ (found to be adequate for the *ab initio* potential), there are 91 $A_{\mathbf{l}_1\mathbf{l}_2\mathbf{l}}(R)$ coefficients to be determined, of which 56 are unique (the other 35 can be determined from symmetry). Of these 56 unique terms, only 25 were used by Bunker *et al.*[13] to fit the intermolecular part of the *ab initio* potential. In a general expansion of the potential, all 56 terms will be nonzero, although many may be negligibly small [as will be the case for the $(DCl)_2$ expansion].

XI. RESULTS

A. Fully coupled four-dimensional variational method

We report the complete results of the four-dimensional calculation using the *ab initio* analytical potential[13] in order to provide standards by which to compare the approximate techniques described above as well as to completely elucidate the discrepancies with the available spectroscopic results (which are addressed fully in Paper II). Using a basis set of $j_{\max}=9$ and $n=3$, the results for the $J=0$ and $J=1$ levels of $(HCl)_2$ and $(DCl)_2$ calculated from the *ab initio* potential are presented in Table VII. The $J=0$ levels for $(HCl)_2$ were previously calculated with a close-coupling method[14] and are in good agreement with the values reported here. Since all 91 $(DCl)_2$ potential coefficients (for an expansion up to $\mathbf{l}_1^{\max}=\mathbf{l}_2^{\max}=5$) are nonzero and must be determined by three-dimensional numerical integration (at each necessary value of R) and because the matrix setup time depends linearly on the number of potential coefficients, the calculation of energy levels for $(DCl)_2$ is much more expensive than the same calculation for $(HCl)_2$. In order to prove the necessity of determining rigorously correct $(DCl)_2$ coefficients, Table VIII shows the results (using a smaller basis set) for selected spectroscopic properties using both the rigorous $(DCl)_2$ coefficients and the untransformed $(HCl)_2$ coefficients. It is clearly seen that the differences in the two calculations are unacceptably large, given the desire to quantitatively compare these energies to the very accurately measured spectroscopic data.

In Table IX, we present results for the mixed dimer (HCl)(DCl) based on the *ab initio* potential (using rigorously determined potential coefficients). In addition to the effort required to determine the potential coefficients, the loss of permutation symmetry and the resulting increase in the size of the matrices makes the calculation of these energy levels difficult. A basis set size of $j_{\max}^{\mathrm{HCl}}=j_{\max}^{\mathrm{DCl}}=8$ and only one radial basis function was used.

In addition, the loss of symmetry makes the assignment of the eigenstates difficult—we simply assign a numerical label to each $J=0$ state. In order to aid in making this assignment, expectation values of $\langle P_1(\cos\theta)\rangle$ and $\langle P_2(\cos\theta)\rangle$ and relative absorption intensities (for the $J=0\rightarrow1$ transitions originating from the lowest eigenstate and normalized to the largest value) were also calculated. From the expectation values, it is apparent that the ground state has an average geometry with the DCl subunit as the hydrogen bond donor, while the first excited state has the HCl subunit as the hydrogen bond donor. The assignment of other states is unclear, although the relative absorption intensities provide an indication of the more strongly allowed transitions.

B. Approximations

In Table X, results obtained with the various approximate methods are compared with each other and with the exact 4D results for calculations using the analytical *ab initio* potential of Bunker *et al.*[13] A similar comparison for calculations using the experimental ES1 potential described in the accompanying paper is presented in Table XI.

C. Semirigid bender

In Table X, the results for the semirigid bender calculations are presented in two columns, labeled ''pure'' and ''fit''. The results using the one dimensional tunneling poten-

TABLE VII. Calculated energy levels from *ab initio* (Ref. 13) potential surface (in cm^{-1}).

	$(H^{35}Cl)_2$		$(D^{35}Cl)_2$	
Assignment	$J=0$	$J=1$	$J=0$	$J=1$
	A^+ symmetry	B^- symmetry	A^+ symmetry	B^- symmetry
$\|0\ 0\ 0\ 0\rangle K_a=0$	−373.138 71	−373.017 44	−424.970 95	−424.850 55
$\|0\ 0\ 0\ 0\rangle K_a=1^-$		−362.061 78		−419.388 06
$\|0\ 1\ 0\ 0\rangle K_a=0$	−324.601 13	−324.484 63	−373.393 42	−373.277 80
$\|0\ 0\ 2\ 0\rangle K_a=0$	−314.045 47	−313.924 91	−385.478 55	−385.358 08
$\|0\ 1\ 0\ 0\rangle K_a=1^-$		−313.452 00		−367.866 37
$\|0\ 0\ 2\ 0\rangle K_a=1^-$		−303.911 35		−380.266 07
$\|0\ 2\ 0\ 0\rangle K_a=0$	−278.778 66	−278.667 18	−324.680 49	−324.568 14
$\|0\ 2\ 0\ 0\rangle K_a=1^-$		−267.560 13		−319.267 06
$\|0\ 1\ 2\ 0\rangle K_a=0$	−266.913 12	−266.797 47	−337.753 08	−337.636 58
$\|0\ 1\ 2\ 0\rangle K_a=1^-$		−256.591 13		−332.490 79
$\|0\ 0\ 4\ 0\rangle K_a=0$	−231.419 96	−231.300 78	−329.661 95	−329.544 04
$\|0\ 0\ 4\ 0\rangle K_a=1^+$		−222.817 91		−324.885 95
$\|0\ 2\ 2\ 0\rangle K_a=0$	−222.643 27	−222.530 57	−291.363 26	−291.249 80
$\|0\ 2\ 2\ 0\rangle K_a=1^-$		−212.021 53		−286.072 35
$\|0\ 0\ 1\ 1\rangle K_a=1^+$		−204.927 77		−305.893 03
$\|0\ 1\ 4\ 0\rangle K_a=0$	−187.744 52	−187.630 62	−280.673 91	−280.559 70
$\|0\ 1\ 4\ 0\rangle K_a=1^+$		−178.903 91		−275.896 27
$\|0\ 0\ 6\ 0\rangle K_a=0$	−168.082 57	−167.967 91	−260.213 88	−260.097 48
$\|0\ 1\ 1\ 1\rangle K_a=1^+$		−163.126 55		−259.810 79
$\|1\ 0\ 0\ 0\rangle K_a=0$	−155.174 68	−155.058 80	−265.253 72	−265.136 65
$\|0\ 0\ 6\ 0\rangle K_a=1^+$		−153.014 83		−253.625 04
$\|1\ 0\ 0\ 0\rangle K_a=1^-$		−146.971 90		−260.885 06
	A^- symmetry	B^+ symmetry	A^- symmetry	B^+ symmetry
$\|0\ 0\ 1\ 0\rangle K_a=1^+$		−349.603 90		−415.727 88
$\|0\ 1\ 1\ 0\rangle K_a=1^+$		−299.998 18		−364.644 41
$\|0\ 0\ 3\ 0\rangle K_a=1^+$		−264.881 71		−356.676 22
$\|0\ 2\ 1\ 0\rangle K_a=1^+$		−253.250 38		−316.382 47
$\|0\ 0\ 0\ 1\rangle K_a=0$	−237.082 98	−236.964 66	−318.704 32	−318.585 91
$\|0\ 0\ 0\ 1\rangle K_a=1^-$		−225.568 30		−313.080 38
$\|0\ 1\ 3\ 0\rangle K_a=1^+$		−218.217 32		−306.845 37
$\|0\ 1\ 0\ 1\rangle K_a=0$	−195.315 60	−195.201 98	−279.214 09	−279.095 49
$\|0\ 1\ 0\ 1\rangle K_a=1^-$		−184.128 66		−274.233 22
$\|0\ 0\ 5\ 0\rangle K_a=1^+$		−182.696 86		−293.099 86
$\|0\ 2\ 3\ 0\rangle K_a=1^+$		−174.093 23		−261.762 38
$\|0\ 0\ 2\ 1\rangle K_a=0$	−170.454 15	−170.335 79	−272.533 76	−272.419 97
	B^+ symmetry	A^- symmetry	B^+ symmetry	A^- symmetry
$\|0\ 0\ 1\ 0\rangle K_a=0$	−360.705 89	−360.584 91	−421.337 33	−421.217 19
$\|0\ 0\ 1\ 0\rangle K_a=1^-$		−349.604 34		−415.728 70
$\|0\ 1\ 1\ 0\rangle K_a=0$	−311.213 41	−311.097 35	−370.279 15	−370.162 86
$\|0\ 1\ 1\ 0\rangle K_a=1^-$		−299.998 59		−364.645 23
$\|0\ 0\ 3\ 0\rangle K_a=0$	−274.930 14	−274.810 11	−361.780 56	−361.661 75
$\|0\ 0\ 3\ 0\rangle K_a=1^-$		−264.882 11		−356.677 06
$\|0\ 2\ 1\ 0\rangle K_a=0$	−264.566 83	−264.455 11	−321.993 14	−321.880 20
$\|0\ 2\ 1\ 0\rangle K_a=1^-$		−253.250 76		−316.383 25
$\|0\ 1\ 3\ 0\rangle K_a=0$	−228.874 85	−228.759 97	−312.065 25	−311.950 35
$\|0\ 0\ 0\ 1\rangle K_a=1^+$		−225.567 78		−313.079 65
$\|0\ 1\ 3\ 0\rangle K_a=1^-$		−218.217 60		−306.846 10
$\|0\ 0\ 5\ 0\rangle K_a=0$	−190.655 84	−190.537 48	−297.913 25	−297.795 32
$\|0\ 2\ 3\ 0\rangle K_a=0$	−185.284 00	−185.170 25	−267.353 63	−267.240 82
$\|0\ 1\ 0\ 1\rangle K_a=1^+$		−184.128 14		−274.232 06
$\|0\ 0\ 5\ 0\rangle K_a=1^+$		−182.696 26		−293.100 22
$\|0\ 2\ 3\ 0\rangle K_a=1^-$		−174.093 47		−261.763 06
	B^- symmetry	A^+ symmetry	B^- symmetry	A^+ symmetry
$\|0\ 0\ 0\ 0\rangle K_a=1^+$		−362.061 21		−419.387 12
$\|0\ 1\ 0\ 0\rangle K_a=1^+$		−313.451 47		−367.865 49
$\|0\ 0\ 2\ 0\rangle K_a=1^+$		−303.910 81		−380.265 00
$\|0\ 2\ 0\ 0\rangle K_a=1^+$		−267.559 57		−319.266 24
$\|0\ 1\ 2\ 0\rangle K_a=1^+$		−256.590 63		−332.489 76
$\|0\ 0\ 4\ 0\rangle K_a=1^-$		−222.818 37		−324.885 26
$\|0\ 0\ 1\ 1\rangle K_a=0$	−216.077 07	−215.958 36	−311.400 67	−311.282 39
$\|0\ 2\ 2\ 0\rangle K_a=1^+$		−212.021 07		−286.071 41
$\|0\ 0\ 1\ 1\rangle K_a=1^-$		−204.928 06		−305.893 87
$\|0\ 1\ 4\ 0\rangle K_a=1^-$		−178.904 52		−275.895 76
$\|0\ 1\ 1\ 1\rangle K_a=0$	−173.377 03	−173.263 24	−265.338 30	−265.224 44
$\|0\ 1\ 1\ 1\rangle K_a=1^-$		−163.126 72		−259.811 64

TABLE VIII. Comparison of $(DCl)_2$ calculations using the rigorously determined *ab initio* (Ref. 13) potential coefficients and the approximate $(HCl)_2$ coefficients (energies in cm^{-1} and relative to ground state).

	Rigorous	Approximate
Ground state $J=1$	0.120 38	0.118 30
Ground state $J=1K_a=1^-$	5.580	5.570
$\|0\ 0\ 1\ 0\rangle$	3.971	4.197
$\|0\ 0\ 2\ 0\rangle$	39.874	39.326

tial (V_{min}) determined from the analytical *ab initio* surface are presented in the pure column. Based on the discrepancies with experiment apparent in these results, Bunker *et al.* added a term to V_{min} in order to account for a possible breakdown in the model: the difference in zero-point energies at the potential minimum and the C_{2h} transition state.[13] The following term (with adjustable parameters) was added:

$$V_{adjust}=-a\ \exp[-5.0(\rho-\pi/2)^2]-(b+c\ \sin\ \rho). \qquad (24)$$

The values of a, b, and c were adjusted in a least-squares fit to the then existing experimental data-only $\nu_5=1$ $K=0-4$ for $(HCl)_2$.[31–33] The results using this adjusted potential ($a=37.38\ cm^{-1}$, $b=4.91\ cm^{-1}$, and $c=-6.82\ cm^{-1}$) are presented in the column labeled fit. The results for both the pure and fit versions of V_{min} are in good agreement with the exact 4D results for the *ab initio* potential, with the V_{adjust} term bringing the $|0\ 0\ 1\ 0\rangle$ state into much better agreement with experiment, although not into better agreement with the fully coupled results for the pure *ab initio* results.

In Table XI, the results for the V_{min} directly determined from the experimental potential surface [which accurately reproduces all experimentally observed eigenstates for both $(HCl)_2$ and $(DCl)_2$] are presented. It is seen that the results for this potential are in rather poor agreement with the fully coupled calculations. In a manner similar to that described above, we attempted to find a one-dimensional potential representation that could reproduce both the experimentally observed $(HCl)_2$ and $(DCl)_2$ spectra for $\nu_5=1$ and 2.[31–35] Although the new data definitely indicated a lower effective barrier than that present in either the pure or fit V_{min}, no single potential could be found to fit the data satisfactorily (even though the differences in zero point energy were considered). Considering only the $(HCl)_2$ data, the fit indicated an effective potential with a barrier of $\sim 20\ cm^{-1}$. The one-dimensional potentials are pictured in Fig. 3. These results indicate a substantial breakdown of the semirigid bender model, which is probably due to coupling of the interchange coordinate to the radial or torsional degrees of freedom, since the experimental data are actually fit (using the fully coupled method) to a 4D potential with a donor–acceptor interchange barrier of 48 cm^{-1} as described in Paper II.

TABLE IX. Energy levels, expectation values, and relative absorption intensities ($J=0\rightarrow1$ transitions originating from ground state) for (HCl)(DCl) using *ab initio* (Ref. 13) potential.

State	K_a	E (cm^{-1})	$\langle P_1\rangle_1$[a]	$\langle P_2\rangle_1$	$\langle P_1\rangle_2$	$\langle P_2\rangle_2$	$I_i\leftarrow1$[b]
1	0	−402.0	0.051	0.325	−0.884	0.710	0.0007
	1	−391.6					1.0000
2	0	−383.3	0.811	0.609	−0.112	−0.297	0.5190
	1	−337.2					0.6478
3	0	−350.1	0.403	0.115	−0.515	0.234	0.6778
	1	−343.4					0.9566
4	0	−319.9	0.436	0.260	−0.347	0.170	0.1340
	1	−314.0					0.0575
5	0	−288.6	0.016	−0.336	−0.831	0.566	0.0000
	1	−280.5					0.0797
6	0	−283.8	0.366	0.240	−0.329	0.222	0.0000
	1	−271.5					0.6391

[a]$\langle P_j\rangle_i$ signifies the expectation value of the jth Legendre polynomial for the ith subunit: 1=HCl, 2=DCl.
[b]Transition intensities normalized to largest values.

TABLE X. Comparison of $(HCl)_2$ eigenstates (energies in cm^{-1} and relative to ground state) calculated with the approximate methods using *ab initio* (Ref. 13) potential.

	1D radial[a]		1D tunneling[a]		3D angular	
$\|\nu_3\nu_4\nu_5\nu_6\rangle$	Cut	Ang	Pure	Fit	$R=3.82$ Å	Full 4D
$\|0\ 0\ 1\ 0\rangle$			8.4	15.5	12.2	12.4
$\|0\ 1\ 0\ 0\rangle$	54.2	48.2				48.5
$\|0\ 0\ 2\ 0\rangle$			60.6	58.9	60.5	59.1
$\|0\ 2\ 0\ 0\rangle$	104.8	91.9				94.4
$\|0\ 0\ 3\ 0\rangle$			98.3	103.2	100.7	98.2
$\|0\ 0\ 0\ 1\rangle$					145.3	136.0
$\|0\ 0\ 1\ 1\rangle$					166.0	157.1
$\|1\ 0\ 0\ 0\rangle$					223.6	218.0

[a]See the text for discussion of subheadings.

D. Reversed adiabatic approximation

1. One-dimensional radial calculation

Because of the small degree of angular–radial coupling exhibited in the *ab initio* surface, the 1D radial calculation using the effective potential constructed from 3D angular energies [$V_{eff}^{ang}(R)$] provides very accurate [with respect to exact calculations using the same $(HCl)_2$ *ab initio* surface] estimates of the fully coupled stretching states ($\nu_4=1$ and 2). The results from the 1D radial calculation using the more approximate $V_{eff}^{cut}(R)$ are less impressive, due to the neglect of the large vibrational averaging evident in the angular coordinates.

TABLE XI. Comparison of $(HCl)_2$ eigenstates (energies in cm^{-1} and relative to ground state) calculated with the approximate methods using experimental ES1 potential.

	1D radial[a]			3D angular		
$\|\nu_3\nu_4\nu_5\nu_6\rangle$	Cut	Ang	1D tunneling	3.75 Å	3.65 Å	Full 4D
$\|0\ 0\ 1\ 0\rangle$			11.5	15.6	27.6	15.7
$\|0\ 1\ 0\ 0\rangle$	74.6	60.9				72.1
$\|0\ 0\ 2\ 0\rangle$			62.0	62.4	72.0	53.3
$\|0\ 2\ 0\ 0\rangle$	142.3	118.2				135.9
$\|0\ 0\ 3\ 0\rangle$			102.6	104.3	116.8	103.9
$\|0\ 0\ 0\ 1\rangle$				167.1	170.1	160.6
$\|0\ 0\ 1\ 1\rangle$				193.8	210.0	185.1
$\|1\ 0\ 0\ 0\rangle$				231.5	235.9	240.8

[a]See the text for discussion of subheadings.

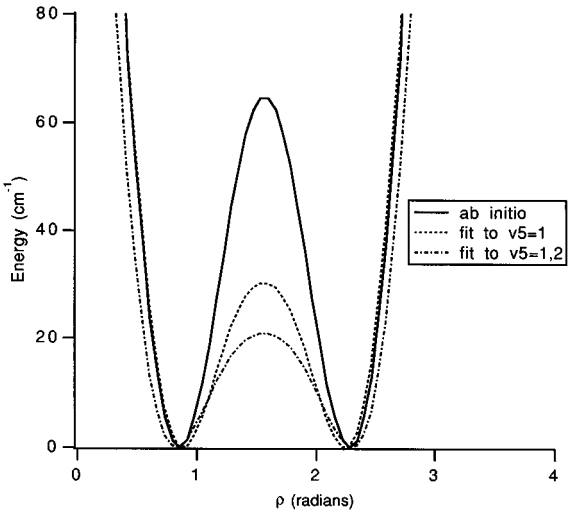

FIG. 3. *Ab initio* and fitted semirigid Bender tunneling potential energy surfaces.

The much more extensive angular-radial coupling evident in the experimental ES1 potential energy surface is manifested in the much worse agreement of the one-dimensional results with the fully coupled calculations. In particular, the effective potential constructed by 3D angular energies $[V_{\text{eff}}^{\text{ang}}(R)]$ actually produces worse agreement with the fully coupled results than does the simpler 1D potential cut method.

E. Reversed adiabatic approximation

1. Three-dimensional angular method

For reversed adiabatic calculations using the *ab initio* potential, the intermolecular distance (R) was fixed at 3.82 Å, the minimum in the potential surface along the entire donor–acceptor interchange tunneling pathway. For calculations using our ES1 surface, the intermolecular distance was fixed at two different distances—3.75 and 3.65 Å—the equilibrium distances for the hydrogen bonded structure (equilibrium) and the C_{2h} (top of tunneling barrier) structures, respectively.

By reference to Table X, it is seen that the three-dimensional calculation results obtained with the *ab initio* potential are very impressive when compared to the fully coupled results, indicating the quite good quantitative accuracy of this method for this *particular* potential energy surface. However, the results in Table XI indicate that the reversed adiabatic angular approximation (RAA) method is very sensitive to the choice for fixed R for the experimental potential, and provides a much less quantitative estimate of the energies when compared to the exact results. Hence, the validity of this widely used approximation is highly system dependent, and results obtained with it should be very carefully examined.

XII. SUMMARY

We have examined a hierarchy of approximate calculations for the vibration–rotation–tunneling spectra for $(HCl)_2$ ranging from one-dimensional models to a fully coupled four-dimensional treatment of the intermolecular dynamics. We have also reported the results from fully coupled four-dimensional calculations of $(HCl)_2$ using an analytical *ab initio* surface[13] extended to the deuterated isotopomers and to total angular momentum states greater than zero. These calculations were used to facilitate comparisons with the approximate methods of lower dimensionality as well as allow a complete comparison with the available experimental results (as elucidated in the accompanying paper). The most important conclusion arising from this work is the quantitative demonstration that the validity of the various approximate models is extremely system specific. We used two different potentials for $(HCl)_2$—an *ab initio*[13] and the ES1 experimental surface described in the accompanying paper—and found that the approximate methods were much more accurate for the *ab initio* potential. All of the approximate methods addressed in this paper were found to be highly sensitive to the approximate separability of the radial and angular degrees of freedom, which is the primary difference between the two potentials. Of particular importance, the commonly used reversed adiabatic angular approximation was found to be very sensitive to the choice for fixed R; an improper choice would lead to results very much different from the fully coupled results and undoubtedly to false conclusions concerning the intermolecular potential energy surface. We have also addressed the neglect of Coriolis coupling terms, and the necessity of performing a proper coordinate transformation for the calculation of spectra for the $(HCl)_2$ isotopomers. Both of these considerations are of substantial magnitude such that a fully quantitative treatment intended to quantitatively describe high resolution spectroscopic VRT data of $(HCl)_2$ absolutely requires their rigorous inclusion. In the accompanying paper we describe the determination of the experimental potential surface used to demonstrate the limitations of the approximate methods in this paper. This potential was generated by the least-squares fitting of a detailed analytical form for the potential to the complete body of available spectroscopic data for $(HCl)_2$ and $(DCl)_2$, necessarily employing the highest levels of theory described in this paper for the calculation of the relevant eigenstates.

ACKNOWLEDGMENTS

The authors are grateful for helpful discussions with Kun Liu. This work was supported by the Experimental Physical Chemistry Program of the National Science Foundation (Grant No. CHE-9123335).

[1] R. J. LeRoy and J. M. Hutson, J. Chem. Phys. **86**, 837 (1987); R. J. LeRoy, C. Bissonnette, J. Wu, A. Dham, and W. Meath, Faraday Discuss. Chem. Soc. **97**, 81 (1994).
[2] J. M. Hutson, J. Chem. Phys. **96**, 6752 (1992); J. Phys. Chem. **96**, 4237 (1992).
[3] M. Quack and M. A. Suhm, J. Phys. Chem. **95**, 28 (1991).
[4] L. Dore, R. C. Cohen, C. A. Schmuttenmaer, K. L. Busarow, M. J. Elrod, J. G. Loeser, and R. J. Saykally, J. Chem. Phys. **100**, 863 (1994).
[5] A. R. Cooper and J. M. Hutson, J. Chem. Phys. **98**, 5337 (1993).
[6] J. W. I. van Bladel, A. van der Avoird, P. E. S. Wormer, and R. J. Saykally, J. Chem. Phys. **97**, 4750 (1992).
[7] E. H. T. Olthof, A. van der Avoird, and P. E. S. Wormer, J. Chem. Phys. **101**, 8430 (1994).

[8] S. C. Althorpe and D. C. Clary, J. Chem. Phys. **102**, 4390 (1995); **101**, 3603 (1994).
[9] C. Leforestier (private communication).
[10] R. C. Cohen and R. J. Saykally, J. Chem. Phys. **98**, 6007 (1993).
[11] C. A. Schmuttenmaer, R. C. Cohen, and R. J. Saykally, J. Chem. Phys. **101**, 146 (1994).
[12] A. Karpfen, P. R. Bunker, and P. Jensen, Chem. Phys. **149**, 299 (1991).
[13] P. R. Bunker, V. C. Epa, P. Jensen, and A. Karpfen, J. Mol. Spectrosc. **146**, 200 (1991).
[14] P. Jensen, M. D. Marshall, P. R. Bunker, and A. Karpfen, Chem. Phys. Lett. **187**, 594 (1991).
[15] S. C. Althorpe, D. C. Clary, and P. R. Bunker, Chem. Phys. Lett. **187**, 345 (1991).
[16] M. D. Schuder, C. M. Lovejoy, R. Lascola, and D. J. Nesbitt, J. Chem. Phys. **99**, 4346 (1993).
[17] M. D. Schuder, D. D. Nelson, Jr., and D. J. Nesbitt, J. Chem. Phys. **99**, 5045 (1993).
[18] J. T. Hougen, P. R. Bunker, and J. W. C. Johns, J. Mol. Spectrosc. **34**, 136 (1970).
[19] S. C. Ross and P. R. Bunker, J. Mol. Spectrosc. **101**, 199 (1983).
[20] P. R. Bunker and J. M. R. Stone, J. Mol. Spectrosc. **41**, 310 (1972).
[21] P. R. Bunker and B. M. Landsberg, J. Mol. Spectrosc. **67**, 374 (1977).
[22] P. R. Bunker, B. M. Landsberg, and B. P. Winnewisser, J. Mol. Spectrosc. **74**, 9 (1979).
[23] P. R. Bunker and D. J. Howe, J. Mol. Spectrosc. **83**, 288 (1980).
[24] P. R. Bunker, T. Carrington, Jr., P. C. Gomez, M. D. Marshall, M. Kofranek, H. Lischka, and A. Karpfen, J. Chem. Phys. **91**, 5154 (1989).
[25] I. P. Hamilton and J. C. Light, J. Chem. Phys. **84**, 306 (1986).
[26] S. Green, J. Chem. Phys. **62**, 2271 (1975).
[27] R. N. Zare, *Angular Momentum* (Wiley, New York, 1988).
[28] A. G. Ayllon, J. Santamaria, S. Miller, and J. Tennyson, Mol. Phys. **71**, 1043 (1990).
[29] R. J. LeRoy, J. S. Carley, and J. E. Grabenstetter, Faraday Discuss. Chem. Soc. **62**, 169 (1977).
[30] R. Votava, R. Ahlrichs, and A. Geiger, J. Chem. Phys. **78**, 6841 (1983).
[31] G. A. Blake, K. L. Busarow, R. C. Cohen, K. B. Laughlin, Y. T. Lee, and R. J. Saykally, J. Chem. Phys. **89**, 6577 (1988).
[32] G. A. Blake and R. E. Bumgarner, J. Chem. Phys. **91**, 7300 (1989).
[33] N. Moazzen-Ahmadi, A. R. W. McKellar, and J. W. C. Johns, J. Mol. Spectrosc. **138**, 282 (1989).
[34] M. D. Schuder, C. M. Lovejoy, D. D. Nelson, Jr., and D. J. Nesbitt, J. Chem. Phys. **91**, 4418 (1989).
[35] M. J. Elrod and R. J. Saykally, J. Chem. Phys. **103**, 933 (1995).